

---

# Finding faults: Using ground roll reflections to image lateral discontinuities

Craig Hyslop\*, Robert R. Stewart\*, and Minyu Zhang\*

## ABSTRACT

Determining lateral change in the subsurface is important for many scales of geophysical investigation: It is helpful in constraining models for tectonic behavior, structural mapping on a regional scale, characterizing reservoirs, and identifying faults for engineering applications. Surface-seismic survey geometries and reflection processing methods are well suited for imaging horizontal layers in the subsurface; however, illuminating and analyzing near-vertical features and lateral discontinuities may be more difficult. Processing surface waves directly can provide additional information about lateral change in the subsurface. We have developed a processing flow for imaging faults using reflected surface waves. The method relies on VSP-type procedures as well as the undoing of dispersive effects. It provides a way to locate lateral change and the discontinuity depth using extracted surface-wave reflectivity. We apply the method to synthetic datasets generated from a buried fault model and find interpretable images of the fault. Next, we use surface-wave reflectivity for interpreting a near-surface fault in field data from the Hockley Fault system near Houston Texas. We note that a major fault breaks the surface (pavement) at 400m which is identified in the ground-roll image.

## INTRODUCTION

Determining lateral change in the subsurface is important for many scales of geophysical investigation. It is helpful in constraining models for tectonic behavior, structural mapping on a regional scale, characterizing reservoirs, and identifying faults for engineering applications. Surface-seismic survey geometries and reflection processing methods are well suited for horizontal layers in the subsurface; however, near-vertical features and lateral discontinuities require sophisticated algorithms (Hale et al., 1992) and additional sources and receivers placed within the subsurface (Lu et al., 2008). Processing surface waves directly provides additional information about lateral change in the subsurface. Surface wave tomography (Abbott et al., 2006) and phase-velocity inversion (Park et al., 1998) are common surface-wave processing methods that provide a shear-wave velocity model. For exploration-scale surveys, these shear-wave velocity models have proven helpful for static corrections (Dulaijan and Stewart, 2010) and (Dura-Gomez and Zurek, 2011). Shear-wave velocity models from simple surface-wave tomography and surface-wave phase-velocity inversion are also effective in determining smooth lateral discontinuities (Douma and Haney, 2011) and (Roy et al., 2013). A unique method to determine sharp lateral change in the near-surface problem is to image the incident locations of back-reflected surface waves. Similar to imaging with scattered surface-waves, which has been shown to be effective in locating objects in the near-surface (Blonk et al., 1995) and (Herman et al., 2000), lateral reflectivity of surface waves can be extracted once the lateral locations of back-reflected surface waves are known. In addition to providing informa-

---

\*Department of Earth and Atmospheric Sciences, University of Houston

tion about the lateral location of a discontinuity, the frequency spectrum for surface-wave reflectivity provides information about depth to the discontinuity.

In this paper, we assume contrasts conform to boundaries, such as faults which are oblique to the survey line and are at intervals sufficient to create back-reflected surface waves. Given a simple model, locating this type of back-reflection from surface waves can be performed in a rough sense simply by visually inspecting the shot gather. However, for dispersive surfaces waves and complex models, the outgoing wave and other back-reflected waves mask the onset of the back-reflection and reduce the accuracy for identifying the location of the discontinuity and frequency content of reflectivity. Therefore, the primary challenge in locating the incident location of the back-reflected surface wave is in separating the incoming and outgoing wave-field.

To image the incident location for back-reflected surface waves we follow a processing flow is similar to that of a Vertical Seismic Profile (VSP), see (Ross and Shah, 1987), except that our data geometry is horizontal instead of vertical, and there is the added complexity of accounting for a dispersed surface wave. We use a series of phase-velocity matching operations which are an extension of the Fourier time-shift property (Herrmann and Russell, 1990) for the purpose of flattening a surface wave. Determining the correct average phase-velocity model is necessary for flattening the surface-wave. We present a way to invert for the average phase-velocity. Incident locations for back-reflected surface waves are enhanced and the reflectivity spectrum provides a visual way to interpret the location and depth to the discontinuities. We use a deterministic deconvolution of the incoming back-reflected surface wave with the outgoing surface wave to find reflectivity. We show imaging back-reflections are a effective way to characterize lateral discontinuities in the subsurface.

## METHODS

### Forward model

We assume that a shot record,  $D$ , is comprised of traces which have recorded the outgoing surface wave,  $O$ , incoming surface wave,  $I$ , and noise,  $N$ , which also includes all other arrivals.

$$D = O + I + N. \quad (1)$$

Assuming the variables above have been transformed to the frequency domain, an outgoing surface wave propagating across a ray-path to the position of an incident reflection,  $x_i$ , is modeled by:

$$O(\omega, x_i) = M(x_i)A(\omega)e^{-i(k(\omega)x_i - \omega t)}e^{-\alpha\omega x_i}e^{i\phi(\omega, x_i)}, \quad (2)$$

where  $A$  is the source wavelet that exhibits amplitude loss due to geometric spreading,  $M$ , and attenuation,  $\alpha$ . Dispersion due to layering in the near surface and attenuation,  $\phi$ , are also included. Here, wavenumber,  $k$ , is a function of frequency,  $\omega$ , defined by surface-wave dispersion-curves at every location along the ray-path traveled. As shown by (Lee and Ross, 2008) and (Krohn, 2010), the phase shift at each trace is dependent on phase-velocities,  $c(\omega)$ , which are averaged across the path traveled to that trace. Assuming the distance between  $N$  number of receivers is constant,  $dx$ , the phase-shift of a surface wave

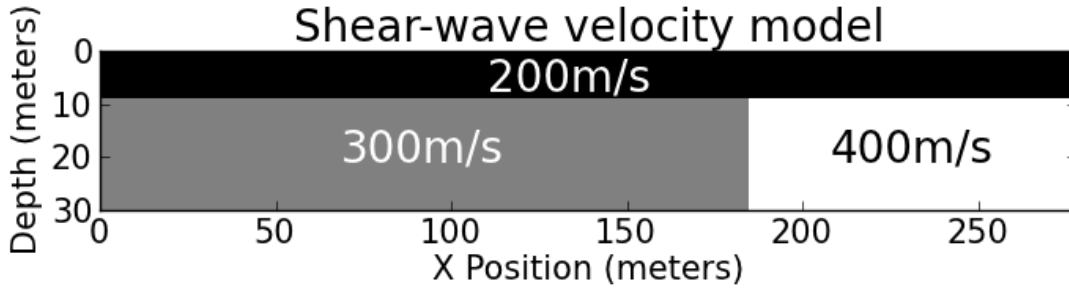


FIG. 1. Shear-wave velocity model used for analytic and numerical solutions of the surface wave.

is defined by,

$$k(\omega)x_i = Ndx \left[ \frac{1}{N} \left( \frac{1}{c(\omega)_1} + \frac{1}{c(\omega)_2} + \frac{1}{c(\omega)_N} \dots \right) \right] \cdot \omega. \quad (3)$$

The incoming wave returning back towards the source along  $x$ , from a incident at  $x_i$  is then:

$$I(\omega, x, x_i) = O(\omega, x_i)R(\omega, x_i)P_I, \quad (4)$$

where  $P_I$  is the propagation term necessary to generate dispersive waves at each trace along the incoming ray-path for the surface wave.

$$P_I = M(x - x_1)e^{-i(k(\omega)x - x_1 - \omega t)} e^{-\alpha\omega x - x_1} e^{i\phi(\omega, x - x_1)} \quad (5)$$

In effect, the outgoing surface wave at the incident location, becomes the new source for the incoming surface-wave propagating in the opposite direction.

We compare our analytic solution for surface wave propagation to synthetic data generated using a continuous Galerkin spectral-element method, SPECFEM2D (Komatitsch and Tromp, 2002). Our shear wave velocity model is comprised of two layers. The first layer has a constant velocity down to a 9 meter depth, and the second layer is split by a vertical fault with a different velocity on either side (Figure 1).

We use a Ricker source with a 10 Hz dominant frequency placed just below the surface to excite surface waves. Vertical component receivers are simulated at a 1 meter spacing along the entire extent of the model. For our analytic forward modeling we generate 1D dispersion-curves,  $c(\omega)$ , at each receiver location and use equation 2 to model the fundamental mode of the outgoing surface-wave. Reflectivity between each receiver is determined by a velocity difference. Figure 2 shows the comparison for an off-end shot of the analytical and spectral element solution.

### Processing flow

Our objective is to recover the reflectivity term,  $R(\omega, x_1)$ , in equation 4 and convert frequency dependent amplitude of reflectivity to depth  $R(\omega, x_1) \rightarrow R(z, x_1)$ . To recover reflectivity we account for dispersion due to layering as well as amplitude loss from geometric spreading and attenuation. We use phase-shifting to account for dispersion due to layering and deconvolution to account for all other amplitude loss. Our processing flow is illustrated using the same model and synthetic data generated by SPECFEM2D in the section above.

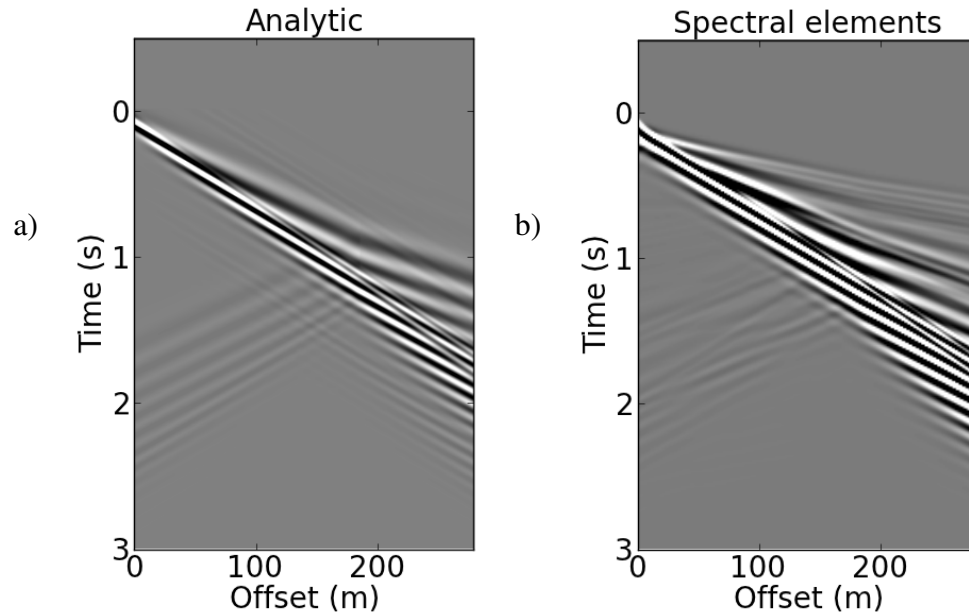


FIG. 2. Comparison of forward model outlined in this paper on the left versus numerical solution via spectral elements on the right. Only the fundamental mode of the surface wave is modeled analytically. The numerical solution represents the full solution of the wave-equation.

#### *Determining the phase-velocity model*

A correctly defined phase-shift will de-disperse, or flatten, the outgoing surface-wave making it possible to design a filter to recover the location of the incident surface wave reflection. However, the average phase-velocity needed to flatten the outgoing wave is unknown. We beamform within spatial windows, pick dispersion curves, and integrate across the ray-path to determine a starting average phase-velocity model for the phase-shift. We then employ a waveform inversion in the flattened domain to find the averaged phase-velocity model which best flattens the data.

Our set of data is the source,  $S$ , and a reverse transfer function,  $H^*$ , based on the propagation terms in equations 2-5, needed to return the dispersed wave to time zero. Note that the source found by returning the dispersed wave to time zero includes transmission effects collected along path traveled. A least-squares inversion can be formulated where the source we are trying to fit is a function of  $H^*$ , and a vector of parameters,  $p$ , that defines the average phase-velocities. We define the parameters using a dispersion curve-fitting function described by (Tang et al., 2009). Our objective is to minimize the error of the sum of the squares of all frequency components. A single source can be extracted from the near offsets as a goal for the flattened surface wave. The inversion improves the alignment and de-dispersion of the outgoing wave. The incoming incident reflections are also better focused. Figure 3 shows the initial flattened data domain and the improved inverted result.

#### *Separating the wave-field*

Once accurate velocities for the phase-shift have been estimated, the incoming and outgoing surface waves are separated using a VSP-type flow. The shot gather is flattened

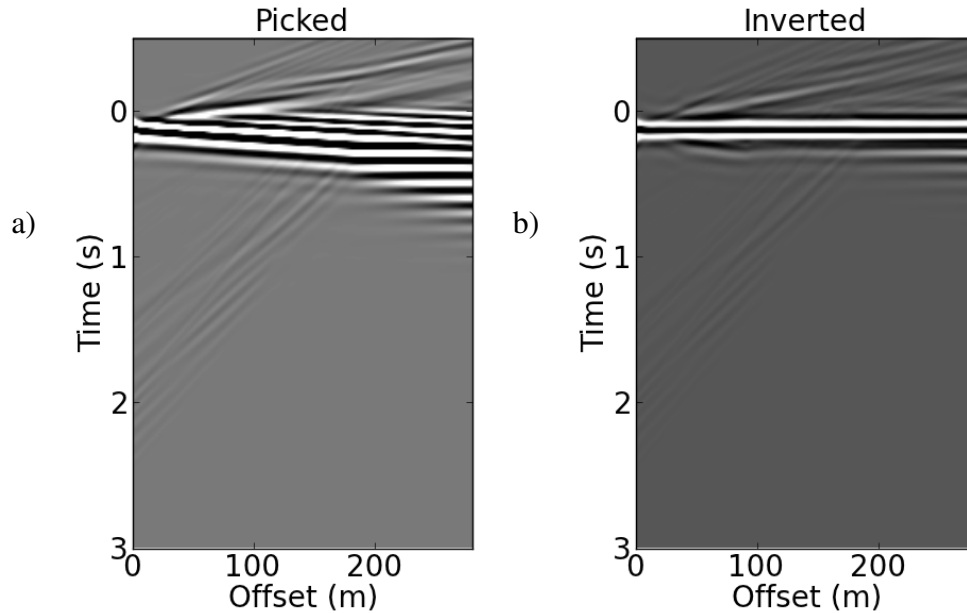


FIG. 3. Initial flattened data using beamformed phase-velocities and inverted result.

using the reverse of the transfer function and the outgoing surface wave is enhanced with a median filter (Figure 4a). Then, the enhanced outgoing surface wave is subtracted from the flattened surface wave resulting in a residual dataset with incoming back-reflected surface waves (Figure 4b).

Along with the expected back-reflection from the fundamental mode of the surface wave there are other back-reflections from higher modes and there are conversions back to body-waves. The majority of surface wave energy is back-reflected from the fundamental mode and a strong higher mode at time that has been over-corrected for flattening.

#### *Imaging lateral reflectivity*

In the flattened domain, both the outgoing and the incident of the incoming wave are de-dispersed for layer effects. At this point we diverge somewhat from the standard VSP flow. It is possible to align the incoming wave at two-way travel time; however, in doing so the aligned incoming wave will exhibit dispersive effects present at two-way travel time for all offsets. Given substantial dispersion, incoming waves will overlap, defeating the purpose of stacking to improve the quality of the reflection. Instead, we stack the incoming wave by back-propagating from zero offset towards zero-time in the flattened domain (Figure 5a). Propagation effects due to geometric spreading and attenuation are removed by deconvolution of the incoming by the outgoing. By deconvolving the data we also account for coupling effects. We use damped deconvolution in the Fourier domain (Claerbout and Fomel, 2006), including both amplitude and phase parts of the data.

$$R(\omega, x) = \frac{O(\omega, x) * I(\omega, x, x)}{O(\omega, x) * O(\omega, x) + \epsilon^2} \quad (6)$$

Incident back-reflections are isolated from the rest of the incoming wave-field by applying a mute around zero time (Figure 5b).

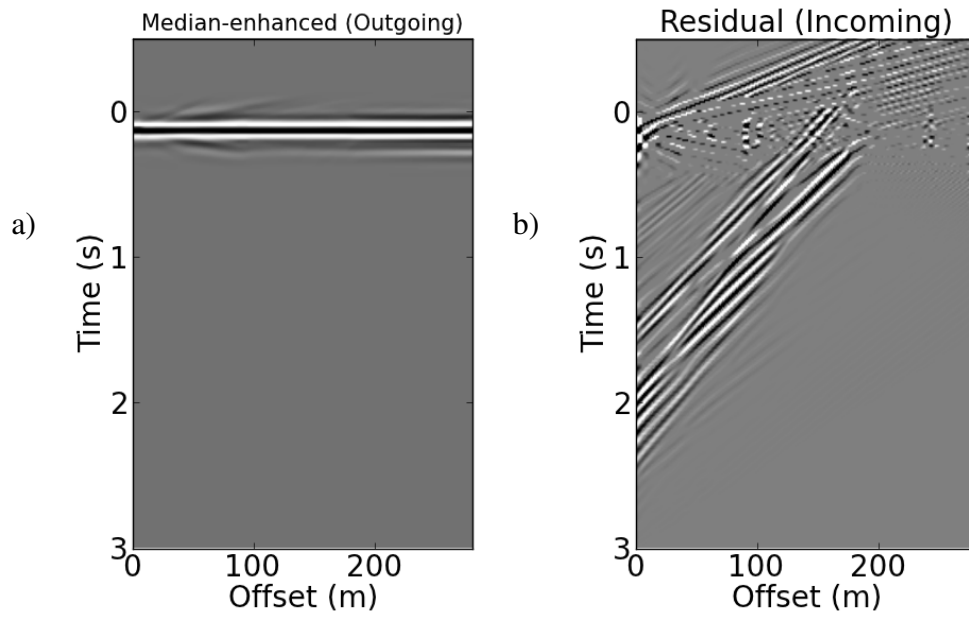


FIG. 4. Median-enhanced flattened data as Outgoing and Residual as Incoming.

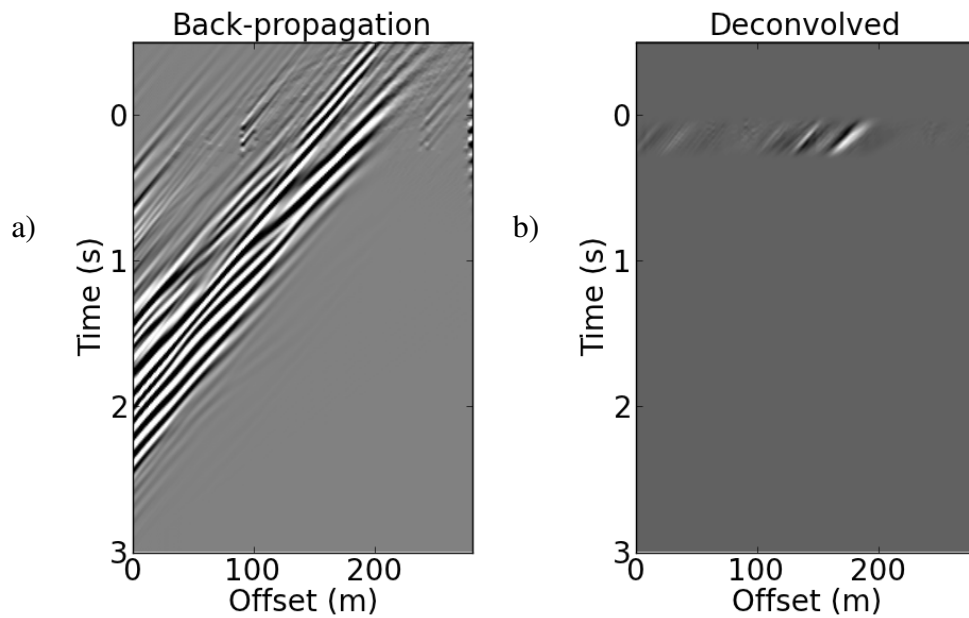


FIG. 5. Back-propagated incoming surface wave and deconvolved result. Incident location of back-reflection is isolated by muting around zero time.

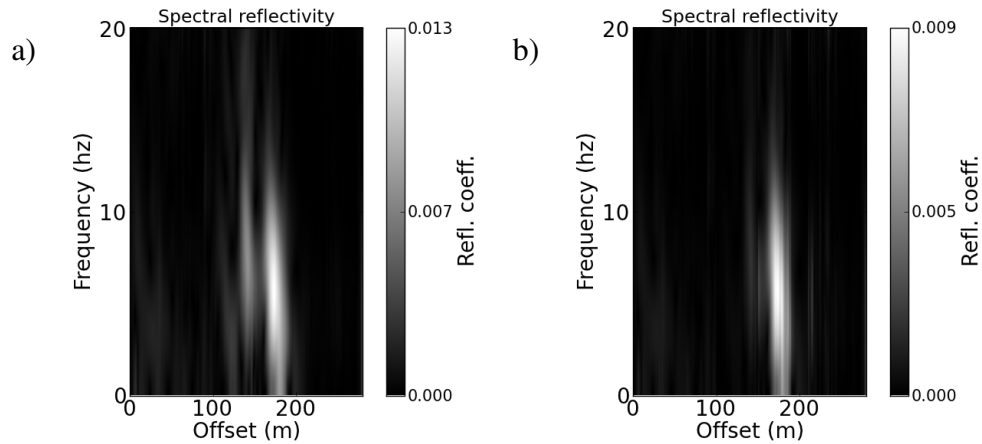


FIG. 6. Reflectivity spectrum determined from single shot, (a). Reflectivity spectrum determined from multiple stacked shots, (b).

Once the mute has been applied the location of back reflections can clearly be seen in both the time domain and the frequency domain (Figure 6a). However, for this shot, there are residual artifacts due to back-reflections from higher modes and conversions back to body-waves back-reflections. Given that propagation effects are now removed by the de-dispersion and deconvolution, the amplitude represents an estimation of reflectivity as a function of frequency.

### *Multi-gather processing*

Incident back-reflections occur at fixed locations on the surface regardless of shot location. There are several ways to combine multiple shots after the incident back-reflections have been deconvolved and isolated. For simplicity, we stack the amplitude part of the shots in the frequency domain. In combining shots, noise, such as back-reflections from higher modes and other conversions, is reduced (Figure 6b).

### *Converting to depth*

It is a general rule-of-thumb that surface waves are most sensitive to the velocity structure at about one-half the wavelength of the surface wave (Rix and Stokoe, 1989). We propose mapping spectral amplitude of reflectivity to an amplitude depth-profile using this same rule-of-thumb. We first create a grid of points corresponding to lateral position and depth. Then, we map the nearest half-wavelength (determined by using the average velocity of the surface-wave) from spectral reflectivity to the grid. The result in an image which shows reflectivity as a function of depth (Figure 7).

## RESULTS

### **Synthetic modeling**

Our shear-wave velocity model includes two examples of blind faults, one deep, with large vertical slip, and the other shallow with small vertical slip (Figure 8). Synthetic data produced by spectral element code SPECFEM2D. Synthetic data is generated using a ricker

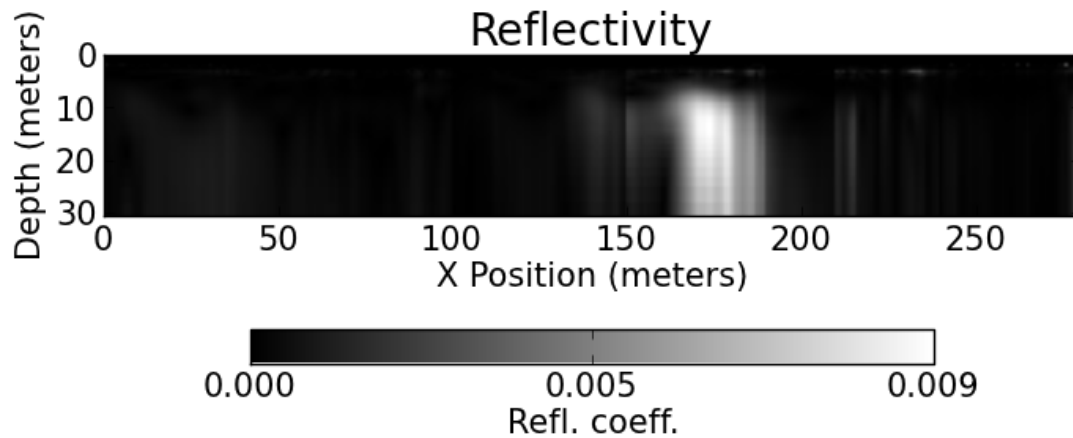


FIG. 7. Image of reflectivity as a function of lateral position and depth.

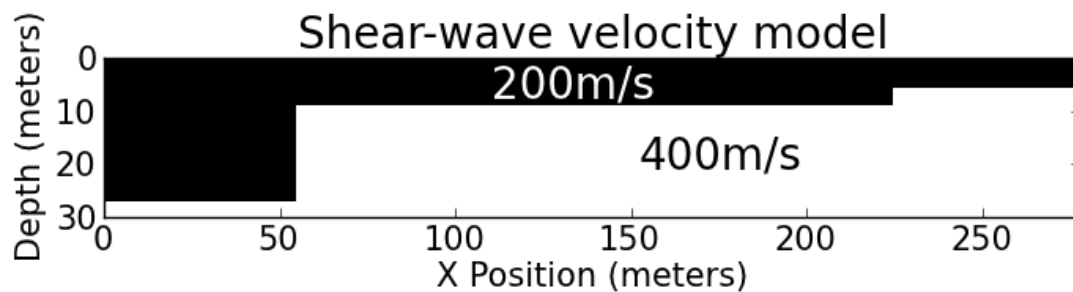


FIG. 8. Shear-wave velocity model used for synthetic testing and split-spread shot generated using SPECFEM2D.

source with a 10Hz dominant frequency. We use split-spread geometry for 14 shots at a 20 meter spacing. Receiver spacing is 1 meter.

Initial estimates for surface-wave phase-velocity are determined using dispersion curves picked from beamforming. Average surface-wave phase-velocities from the beamformed estimates are inverted to flatten and de-disperse the surface wave for outgoing/incoming surface-wave separation. Reflectivity is determined by deconvolving the incoming by the outgoing for all shots. Spectral reflectivity for each shot is determined by isolating incident back-reflections with a mute and transforming to the frequency domain. Finally, spectral reflectivity from all shots are stacked and the result is mapped to depth (Figure 9). Given that the phase and polarity of the back-reflections are accurate, an inversion can be designed to update the velocity model using spectral reflectivity, see Appendix A.

## Field Data

We evaluate the multi-shot processing flow for reflectivity using the Hockley fault in Houston, TX (Khan et al., 2013). The survey was a 2D line recorded with 216 vertical-component geophones at 5m spacing and vertical vibrator sources at the same spacing.

We processed reflection data from the Hockley fault to produce a traditional seismic image. The seismic image shows many vertically oriented faults with a concentration of

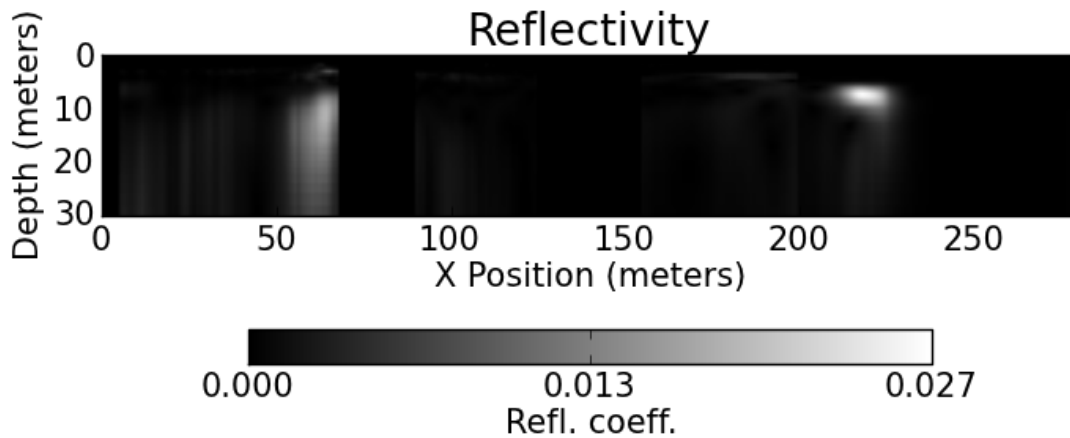


FIG. 9. Reflectivity as a function of depth for synthetic model.

faulting outlined by green circles (Figure 10a). Surface-wave phase-velocities across the lateral extent are determined using dispersion curves picked from beamforming. Each dispersion curve across the 2D-line was inverted to produce the shear-wave velocity model shown in Figure 10b in the background. Note that the frequency content of the surface wave has limited our inversion result to a 25 meter depth. Below that depth shear-wave velocities are extrapolated to the depth of the seismic image.

Using our method, we also processed surface wave data to create spectral amplitude reflectivity images. Spectral reflectivity from all shots are stacked and the result is mapped to depth. The reflectivity image is overlaid on the traditional seismic image in Figure 10c. Note that there is high-amplitude reflectivity near the areas of intense faulting.

## DISCUSSION

Depth of exploration is directly dependent on the wavelength of the surface wave and therefore careful consideration about frequency content of the surface wave and expected velocity properties of the near surface should be taken into account when designing surveys.

It is important to consider that finding unique and accurate dispersion curves across a laterally heterogeneous area is helpful in flattening both the outgoing surface wave and the incoming back-reflected surface wave, as well as improving the frequency-to-depth conversion. Methods based on decomposition of data to determine phase velocity all suffer resolution limits of the receivers used in the decomposition. Therefore, there is the need to increase the resolution and accuracy of the phase-velocities via inversion. For the inversion, care must be taken in selecting the model for the source.

It is encouraging that for our synthetic models reflectivity is large at the fault location and near-zero elsewhere. This is a useful qualitative rule-of-thumb that can be easily used for field data. It is challenging to recover correct reflectivity given noise from higher modes and other converted waves even for synthetic data. Therefore, we refrained from attempting to update the velocity model using reflectivity for the field data. To avoid higher modes and isolate the fundamental mode a filter based on dispersion-curve picks could be applied in  $f$ - $k$  space. Other solutions for reducing noise could include soft-thresholding

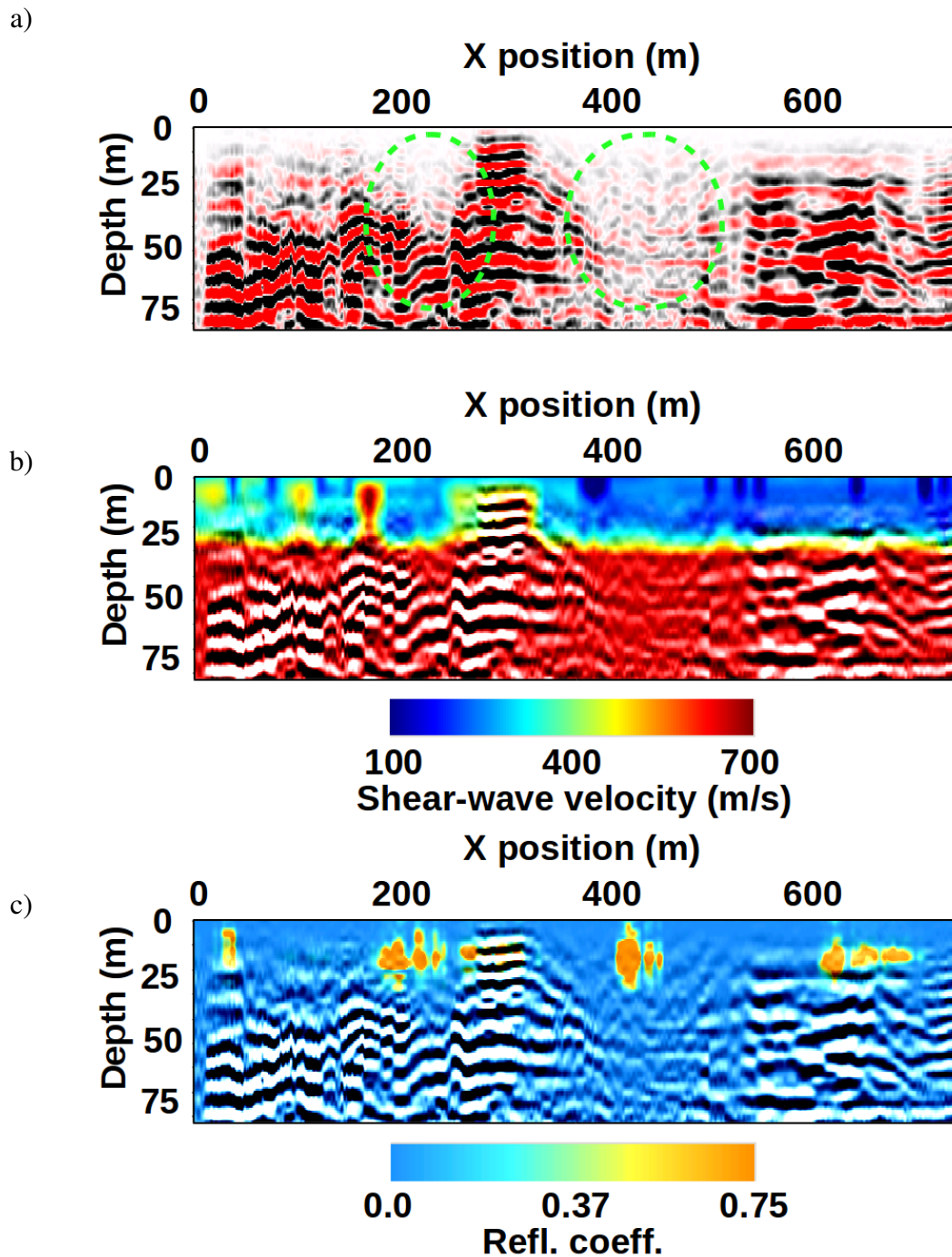


FIG. 10. Images from Hockley fault. Top: Seismic image. Middle: Seismic image with shear-wave velocity model overlay. Bottom: seismic image with reflectivity model overlay.

For our examples, we took the simple approach of combining shots by stacking the amplitude part of the isolated incident back-reflections. Results could be improved by including the phase, or weighting each shot based on its quality.

We also took the simple approach of directly mapping spectral reflectivity to a grid using average velocity of the surface wave. Further study is needed to determine how amplitude of reflected surface waves are related to depth. Potentially, results could be improved by framing an inversion to depth.

Finally, further study is needed about the polarity of back-reflected surface waves. Updating velocity from reflectivity, as it is presented here, depends on a predictable polarity from either a high to low velocity change or a low to high velocity change in the shear-wave velocity model.

## CONCLUSIONS

We have developed a novel processing flow to use reflected surface waves to create subsurface images. The flow has been tested on a number of synthetic and field datasets. Our results indicate that, for frequencies commonly collected by small-scale land surveys, the location and depth to faults can be imaged. Results from the Hockley fault show that reflectivity can be used as an attribute in highlighting the location of faulting, making it a useful tool for interpretation. Provided the survey is well sampled with both sources and receivers, the location of the fault can be resolved with some accuracy. It should be noted that there may be a loss in lateral resolution due to longer wavelengths. Our examples are applicable to the scale of most engineering projects; however, given lower frequencies and higher velocities, the same principles should apply for deeper investigations.

## APPENDIX A

### Updating velocity with reflectivity

We formulate a forward model for reflectivity by assuming a quarter-space model with each side being equivalent to an adjacent source receiver pair,  $i$ , and  $i + 1$ . We determine reflectivity by using a plane-wave estimation for reflectivity within narrow frequency bands. We directly invert for velocity using a method similar to (Lindseth, 1977). Assuming density is constant, and starting with the dispersion model determined from extracting from phase velocities, an update for  $c_{i+1}$  can be determined by solving:

$$c(\omega)_{i+1} = \alpha c(\omega)_i, \quad (7)$$

where,

$$\alpha = \frac{R(\omega)_i + 1}{1 - R(\omega)_i}. \quad (8)$$

This is implemented within a framework of moving windows to stabilize the solution from low frequency drift. Alternatively, a least squares solution can be formulated to stabilize the solution,

$$E = \sum_{j=intervals}^N \|(V_j^{avg} - f(c_j)) + \lambda(R_j - g(c_j))\|^2. \quad (9)$$

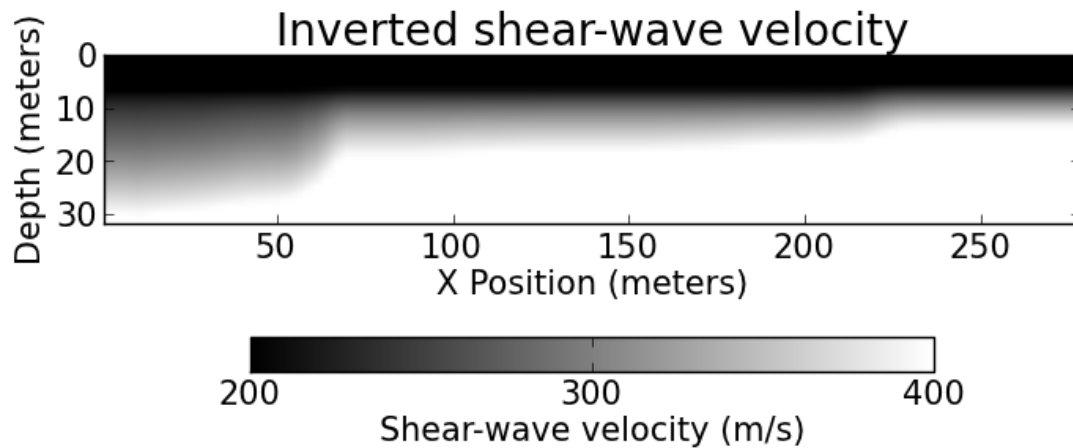


FIG. 11. Shear-wave velocity model updated using reflectivity.

Here, reflectivity,  $R_j$ , is used as a weight to stabilize the first term. The goal is to minimize the errors,  $E$ , given difference between actual average surface-wave phase-velocity,  $V_j^{avg}$  and function of interval surface-wave phase-velocity,  $f(c_j)$ , which predicts  $V_j^{avg}$ . The second term is a weight based on the difference between reflectivity and a function of interval surface-wave phase velocity,  $g(c_j)$ , which predicts reflectivity. Given a large amplitude in the reflectivity term and a correctly specified weight,  $\lambda$ , the second term will allow the first term to dominate the minimization. A reflectivity near zero constricts change introduced by the first term.

Both methods require that polarity of the back-reflections are known. We use data from our two-fault synthetic example and reflectivity to update the shear-wave velocity model. Figure 11 shows results from the direct inversion outlined by equation 8.

## REFERENCES

- Abbott, R. E., Bartel, L. C., Engler, B. P., and Pullammanappallil, S., 2006, Surface-wave and refraction tomography at the FACT Site, Sandia National Laboratories, Albuquerque, New Mexico: Technical Report SAND20065098, Sandia National Laboratories.
- Blonk, B., Herman, G. C., and Drijkoningen, G. G., 1995, An elastodynamic inverse scattering method for removing scattered surface waves from field data: *Geophysics*, **60**, No. 6, 1897–1905.
- Claerbout, J., and Fomel, S., 2006, Image estimation by example: Geophysical Soundings Image Construction, Multidimensional autoregression.  
URL <http://sepwww.stanford.edu/sep/prof>
- Douma, H., and Haney, M., 2011, Surface-wave inversion for near-surface shear-wave velocity estimation at Coronation field: SEG Technical Program Expanded Abstracts 2011, 1411–1415.  
URL <http://dx.doi.org/10.1190/1.3627466>
- Dulaijan, K. A., and Stewart, R. R., 2010, Using surface-wave methods for static corrections: a near-surface study at Spring Coulee, Alberta: SEG Technical Program Expanded

- Abstracts 2010, 1897–1901.  
URL <http://dx.doi.org/10.1190/1.3513212>
- Dura-Gomez, I., and Zurek, B., 2011, 9C 2D Piceance survey: Near-surface velocity model building and tomostatics solution: SEG Technical Program Expanded Abstracts 2011, 1293–1297.  
URL <http://dx.doi.org/10.1190/1.3627440>
- Hale, D., Hill, N. R., and Stefani, J., 1992, Imaging salt with turning seismic waves: Geophysics, **57**, No. 11, 1453–1462.  
URL <http://dx.doi.org/10.1190/1.1443213>
- Herman, G. C., Milligan, P. A., Huggins, R. J., and Rector, J. W., 2000, Imaging shallow objects and heterogeneities with scattered guided waves: Geophysics, **65**, No. 1, 247–252.
- Herrmann, R., and Russell, D., 1990, Ground roll: Rejection using adaptive phase-matched filters: Geophysics, **55**, No. 6, 776–781.  
URL <http://dx.doi.org/10.1190/1.1442890>
- Khan, S. D., Stewart, R. R., Otoum, M., and Chang, L., 2013, Case history. A geophysical investigation of the active Hockley Fault System near Houston, Texas: Geophysics, **78**, No. 4, B177–B185.
- Komatitsch, D., and Tromp, J., 2002, Spectral-element simulations of global seismic wave propagation-I. Validation: Geophysics Journal International, **149**, 390–412.  
URL <http://onlinelibrary.wiley.com/doi/10.1046/j.1365-246X.2002.01653.x/abstract>
- Krohn, C. E., 2010, SWIPER - multi-mode surface wave prediction and removal by waveform matching: 72nd EAGE Conference and Exhibition, P413.  
URL <http://earthdoc.eage.org/publication/publicationdetails/?publication=39873>
- Lee, S., and Ross, W. S., 2008, 3-D mitigation of surface-wave noise in spatially inhomogeneous media: SEG Technical Program Expanded Abstracts 2008, 2561–2565.  
URL <http://dx.doi.org/10.1190/1.3063875>
- Lindseth, R. O., 1977, Mapping stratigraphic traps with Seislog: Proceedings Indonesian Petroleum Association, sixth annual convention, 89–107.
- Lu, R., Willis, M. E., Campman, X., and Toksöz, M. N., 2008, Salt Dome Flank Imaging with Elastodynamic Interferometric Redatuming: SEG Technical Program Expanded Abstracts 2008, 1068–1072.  
URL <http://dx.doi.org/10.1190/1.3059374>
- Park, C. B., Miller, R. D., and Xia, J., 1998, Imaging disperison curves of surface waves on multi-channel record: 68th Annual International Meeting, Society of Exploration Geophysicists, Expanded Abstracts, 1377–1380.  
URL <http://masw.com/files/PAR-98-03.pdf>

- Rix, G., and Stokoe, K., 1989, Stiffness Profiling of Pavement Subgrades: Transportation Research Record No. 1235.
- Ross, W. S., and Shah, P. M., 1987, Vertical seismic profile reflectivity: Ups over downs: *Geophysics*, **52**, No. 8, 1149–1154.  
URL <http://dx.doi.org/10.1190/1.1442379>
- Roy, S., Kocel, E., Dyaur, N., and Stewart, R. R., 2013, Lateral heterogeneity and surface-wave inversion (MASW): SEG Technical Program Expanded Abstracts 2013, 1909–1913.  
URL <http://dx.doi.org/10.1190/segam2013-1084.1>
- Tang, X. M., Li, C., and Patterson, D., 2009, A curve-fitting method for analyzing dispersion characteristics of guided elastic waves: SEG Technical Program Expanded Abstracts 2009.